Journal of Geophysical Research: Atmospheres

RESEARCH ARTICLE
10.1002/2017JD028156

Key Points:
- The hemispheric asymmetric interannual variation of the eastern Pacific ITCZ in the boreal spring is documented
- The interannual variation of ITCZ in the boreal spring is explained by the remote impact of sea surface temperature
- The remote impact of SST on the surface wind convergence causes the interannual ITCZ variation in the eastern Pacific

Supporting Information:
- Supporting Information S1
- Data Set S1

Correspondence to:
M. Zhang,
minghua.zhang@stonybrook.edu

Citation:
Yu, H., & Zhang, M. (2018). Explaining the year-to-year variability of the eastern Pacific Intertropical Convergence Zone in the boreal spring. *Journal of Geophysical Research: Atmospheres*, *123*. https://doi.org/10.1002/2017JD028156

Received 3 DEC 2017
Accepted 21 MAR 2018
Accepted article online 6 APR 2018

Explaining the Year-to-Year Variability of the Eastern Pacific Intertropical Convergence Zone in the Boreal Spring

Haiyang Yu[1] **and Minghua Zhang**[1,2]

[1]School of Marine and Atmospheric Sciences, Stony Brook University, Stony Brook, NY, New York, [2]International Center for Climate and Environmental Sciences/IAP, Chinese Academy of Sciences, Beijing, China

Abstract The year-to-year variability of the Intertropical Convergence Zone (ITCZ) in the eastern tropical Pacific is a significant phenomenon of the tropical climate system. Asymmetric interannual variation of precipitation on two sides of the Equator is often observed there in the boreal spring. We introduce a simple normalized asymmetric index and a double ITCZ index as well as a hierarchical clustering method to describe the ITCZ variation based on the tropical boreal spring precipitation from 1979 to 2017. We show that the indices and the clustering method give consistent categorization of asymmetric ITCZ variation. We find that the asymmetry of precipitation can be explained by the remote impact of the interannual variability of the central Pacific sea surface temperature (SST) on the horizontal gradient of surface pressure and surface wind convergence, especially the Modoki mode. The central Pacific SST also remotely modulates free-tropospheric temperature and vertical stability in the eastern equatorial Pacific, but this remote impact is secondary to the wind convergence. Interannual variability of local SST south of the Equator plays little role in the precipitation variability, which is supported by numerical experiments with a regional atmospheric model. Results imply that surface wind convergence should be considered in convection schemes to improve the simulation of precipitation in the eastern tropical Pacific in climate models.

Plain Language Summary The year-to-year variability of the Intertropical Convergence Zone in the eastern tropical Pacific is a significant phenomenon of the tropical climate system. Maximum precipitation in the boreal spring can be located north of the Equator, south of the Equator, or along the Equator. This study explains why there is such variability in the Intertropical Convergence Zone from 1 year to the other. The remote impact of the large-scale spatial pattern of the sea surface temperature is found to be the cause.

1. Introduction

To a first-order approximation, the spatial distribution of the tropical Pacific (TP) precipitation follows that of the sea surface temperature (SST) (Zhang, 2001). The annual mean precipitation in the eastern Pacific has a maximum zonal band north of the Equator in the Intertropical Convergence Zone (ITCZ) where the maximum SST is located (Figure 1a). During the boreal spring (referring to February, March, and April throughout the present paper), because of the accumulated solar radiation heating and oceanic heat transport (Masunaga & L'Ecuyer, 2010), a secondary zonal band of maximum SST exists in the southeastern equatorial Pacific. Associated with this warm SST is a seasonal transitional maximum of precipitation in the same region in boreal spring (Figure 1b). The boreal spring precipitation in this region, however, varies greatly from year to year (Figures 1c and 1d): double ITCZ occurs in some years but not in other years, and when there is no double ITCZ, a single ITCZ can occur north, south, or at the Equator.

Despite this well-known interannual variability, its mechanism has not been well documented, except for one recent study (Yang & Magnusdottir, 2016) showing that the eastern Pacific ITCZ is possibly related with the central Pacific (CP) El Niño–Southern Oscillation mode. Climate models have been suffering from the "double ITCZ bias" in the equatorial eastern Pacific for more than two decades (e.g., Mechoso et al., 1995; Oueslati & Bellon, 2015; Zhang et al., 2015). In contrast to observations that show only a weak precipitation maximum in a zonal band from 5°S to 15°S in the climatological annual precipitation, many models simulate a maximum there as strong as the maximum north of the Equator (Hwang & Frierson, 2013; Li & Xie, 2014). The reasons for this model bias are still unclear (Oueslati & Bellon, 2015). The large interannual variability of observed precipitation in this region makes the mystery of this model bias more elusive (e.g., Gu et al., 2005; Haffke et al., 2016). A better understanding of this variability is important not only for explaining the interannual variability of the tropical climate system in this region but also for the interpretation of the model differences with observations.

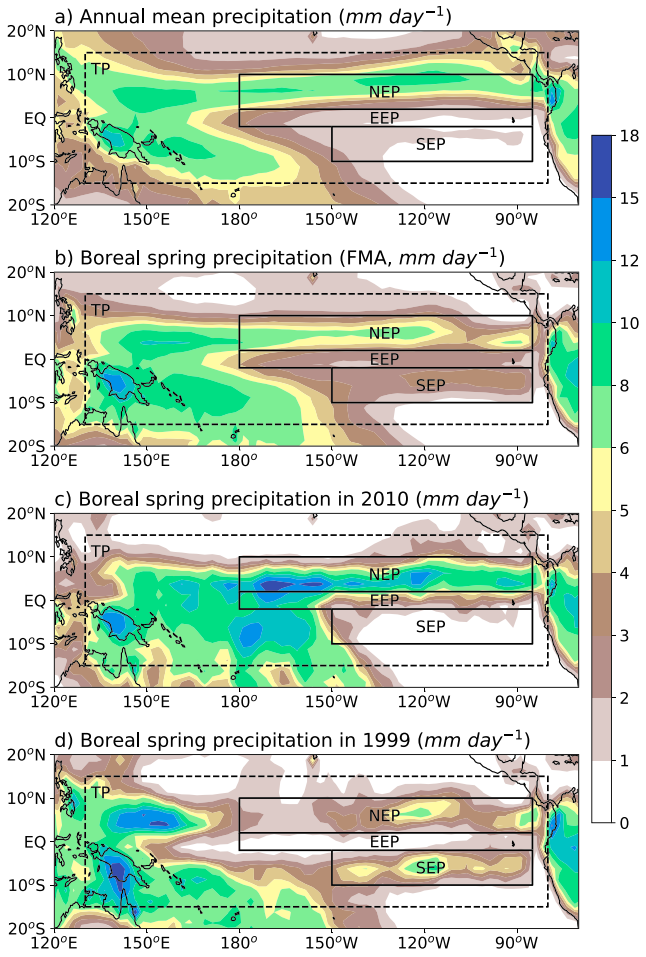

Figure 1. (a) Annual mean precipitation in tropical Pacific (TP, unit: mm/day) from 1979 to 2017. (b) Climatology of boreal spring (February, March, and April) precipitation (unit: mm/day). TP boreal spring precipitation (unit: mm/day) in the year (c) 2010 and (d) 1999. The precipitation is from the monthly Global Precipitation Climatology Project (Adler et al., 2003). The dash rectangle represents the TP domain. The solid rectangles from top to bottom are northeastern equatorial Pacific (NEP), eastern equatorial Pacific (EEP), and southeastern equatorial Pacific (SEP). FMA = February, March, and April.

The objective of this paper is to explain the mechanism of the interannual variability of the boreal spring ITCZ in the equatorial eastern Pacific. In the following, we first describe the observational data, model, and methods in section 2. We then characterize the interannual variability by using two methods and investigate the mechanism in section 3. The last section contains a summary and discussion.

2. Data and Methodology

Observed precipitation, SST, and atmospheric reanalysis data are used in this study. The precipitation is from the monthly Global Precipitation Climatology Project, with a horizontal resolution of 2.5° × 2.5°, from January 1979 to July 2017 (Adler et al., 2003). The SST is from the monthly Extended Reconstructed Sea Surface Temperature version 4 (Huang et al., 2016), with a resolution of 2° × 2° from January 1854 to August 2017. To diagnose the large-scale atmospheric conditions, monthly data from the European Centre for Medium-Range Weather Forecasts Interim Re-Analysis (ERA-Interim) data set (Simmons et al., 2007) are also used, with a resolution of 1.5° × 1.5°, also from January 1979 to June 2017. The variables from ERA-Interim include wind vectors at 10 m, sea level pressure, temperature, humidity, and geopotential height at pressure levels. Surface wind divergence is derived from the wind vectors at 10 m based on the finite-difference method. Monthly Convective Available Potential Energy (CAPE) is derived from the monthly profiles of temperature, humidity, and geopotential height.

To characterize the interannual variability of the eastern Pacific ITCZ during boreal spring, we selected three regions (marked by the solid rectangle boxes in Figure 1a): the northeastern equatorial Pacific (NEP) (180°–85°W, 2°N–10°N); the southeastern equatorial Pacific (SEP) (150°W–85°W, 10°S–2°S), and the eastern equatorial Pacific (EEP) (180°–85°W, 2°S–2°N). We defined two normalized indices to represent the spatial structure of the eastern Pacific ITCZ. These are the asymmetric index (I_a) and double ITCZ index (I_d):

$$I_a = \frac{P_{NEP} - P_{SEP}}{P_m} \tag{1}$$

$$I_d = \frac{P_{NEP} - 2P_{EEP} + P_{SEP}}{P_m} \tag{2}$$

where P is the boreal spring precipitation rate averaged in the domain represented by the respective subscripts, and P_m is the mean precipitation rate in the three regions:

$$P_m = \frac{1}{3}\left(P_{NEP} + P_{EEP} + P_{SEP}\right) \tag{3}$$

The double ITCZ index I_d describes the second-order derivative in the meridional direction of the eastern Pacific precipitation during boreal spring. Negative I_d indicates single precipitation maximum at the Equator, while positive I_d indicates double ITCZs. The asymmetric index I_a distinguishes the preference of the ITCZ to the north ($I_a > 0$) or south ($I_a < 0$) of the Equator (i.e., hemispheric asymmetry), or a symmetric double ITCZ ($I_a = 0$).

Besides the above indices, a hierarchical clustering method is also used on the TP (shown as the dashed box in Figure 1a) precipitation to classify the boreal spring precipitation from 1979 to 2017 into different regimes. In this hierarchical clustering method, the Euclidean distances of the boreal spring precipitation in the TP region between different years are calculated with the cosine of latitude as the weights, and then the classification is made on the order from the minimum distance to the maximum distance as a binary tree (Figure 2b).

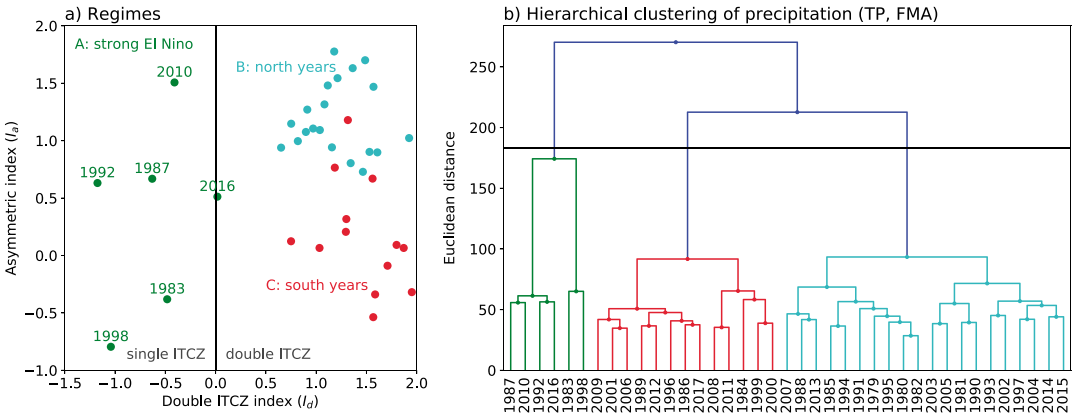

Figure 2. (a) Regime identification of interannual variability of eastern equatorial Pacific precipitation by using the asymmetric index and double ITCZ index. (b) Hierarchical clustering of the boreal spring precipitation in the TP domain. The *x* axis shows the years from 1979 to 2017, and the *y* axis shows the Euclidean distances of precipitation distributions between different years. The black horizontal line represents the 3.5 times of the mean Euclidean distance from the climatology. FMA = February, March, and April; TP = tropical Pacific; ITCZ = Intertropical Convergence Zone.

The Advanced Research Weather Research and Forecasting (WRF-ARW) Version 3.5 model (Skamarock et al., 2008) is used to test the sensitivity of precipitation on dynamics and thermodynamics. Nudging is applied to the WRF to relax the prognostic atmosphere (all model layers from 50 hPa to 1,000 hPa) to the prescribed fields in the 6-hourly ERA-Interim reanalysis data at every time step, with a timescale of 60 min. The simulations are performed in boreal springs from 1979 to 2015. The horizontal resolution is 110 km in both zonal and meridional directions. The Grell and Dévényi (2002) ensemble cumulus parameterization scheme (G3) is used in all simulations.

3. Results

3.1. Interannual Variability of the Eastern Pacific ITCZ During Boreal Spring

The interannual variability of boreal spring precipitation in the TP is characterized by the two indices in Figure 2a. The indices separate different years into three regimes. Regime A has negative values of the double ITCZ index I_d, in which there is a single ITCZ at the Equator. Six years (1983, 1987, 1992, 1998, 2010, and 2016) fall into this regime. They are all strong El Niño years with anomalous warm SST in the eastern equatorial Pacific along the Equator. Most of the years fall into the regimes B and C with positive values of double ITCZ index I_d, in which maximum precipitation is off the Equator. Regimes B and C differ in the asymmetry index, with maximum precipitation anomalies to the north and south of the Equator, respectively. Although the three red dots (corresponding to year 1996, 2008, and 2011) in regime C seem to fall into the regime B as shown in Figure 2a, their precipitation distributions over the TP are similar to regime C except for dry anomalies over the CP during these three years. Since the interannual variation of precipitation associated with strong El Niño events is well understood (e.g., Mason & Goddard, 2001; Ropelewski & Halpert, 1987), we focus on the interannual variability in the two regimes of B and C. We name the regimes B and C as north years and south years, respectively.

The regimes identified above are consistent with classification from the hierarchical clustering method as shown in Figure 2b for regime A (1983, 1987, 1992, 1998, 2010, and 2016), regime B (1979, 1980, 1981, 1982, 1985, 1988, 1990, 1991, 1993, 1994, 1995, 1997, 2002, 2003, 2004, 2005, 2007, 2013, 2014, and 2015), and regime C (1984, 1986, 1989, 1996, 1999, 2000, 2001, 2006, 2008, 2009, 2011, 2012, and 2017). This consistency suggests that the two indices defined in the eastern Pacific are able to describe the general features of the interannual variability of precipitation in the whole TP. This can also be seen in the first mode of empirical orthogonal function (EOF) analysis for all boreal springs of precipitation from 1979 to 2017 as shown in Figures 3a and 3b where the six strong El Niño years in regime A have been excluded. This leading EOF mode explains 39.5% of the variance of boreal spring precipitation in the TP with a specific spatial pattern: positive anomalies north of the Equator in the eastern Pacific are associated with negative anomalies south of the Equator and are accompanied by large areas of precipitation anomalies of the same phase in the western

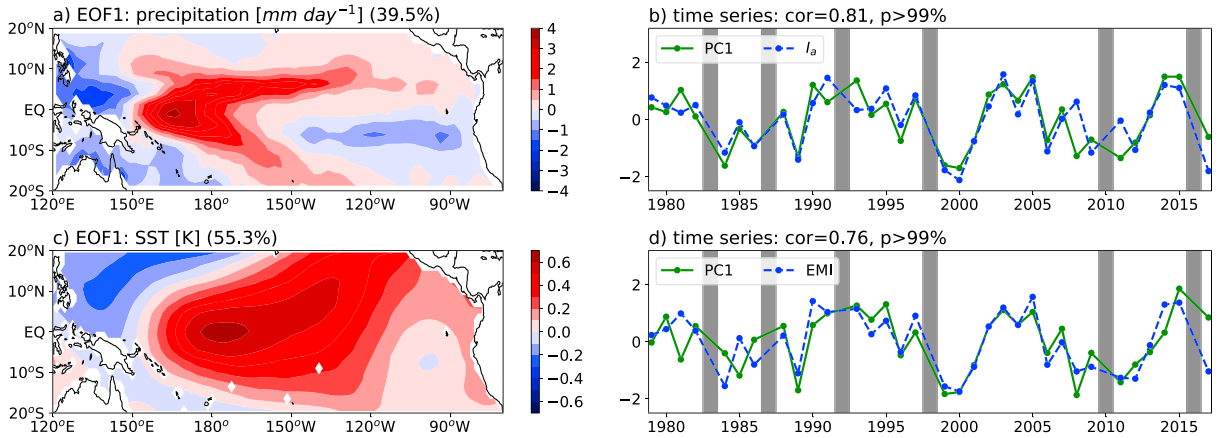

Figure 3. EOF analysis of the boreal spring precipitation (a and b; unit: mm/day) and SST (c and d; unit: K) in the tropical Pacific, excluding the strong El Niño years. The first EOF spatial patterns are shown in Figures 3a and 3c (for precipitation and for SST, respectively) with the percentages of variance contributions in the titles, and the first principal component (PC1) are shown as the solid green lines in Figures 3b and 3d. The dashed blue lines in Figures 3b and 3d represent the normalized asymmetric index of precipitation (I_a) and El Niño–Southern Oscillation mode Modoki index (EMI), respectively. The correlation coefficients and the significant confidences with corresponding PC1 are shown in the titles of Figures 3b and 3d. EOF = empirical orthogonal function; SST = sea surface temperature.

and CP, and vice versa. The corresponding first principal component (PC1) is highly correlated with the asymmetric index I_a of the eastern Pacific precipitation (Figure 3b), with the correlation coefficient (cor) reaching 0.81 and t test probability $p > 99\%$, supporting the notion that the hemispheric asymmetry of the eastern Pacific precipitation during boreal spring in the weak El Niño years is part of the dominant variation of the whole TP precipitation.

This EOF mode of boreal spring precipitation is found to be associated with the first EOF mode of SST in the weak El Niño years. The spatial distribution of the SST mode and the comparison of the PC1 time series of the SST and precipitation modes are shown in Figures 3c and 3d. Positive precipitation anomalies in the NEP are associated with warm SST anomalies with the maxima at the Equator near the dateline and north of the Equator, while positive anomalies in the SEP are associated with the opposite phase of SST anomalies. The correlation coefficient of the PC1 in precipitation and SST is significantly large (cor = 0.79, $p > 99\%$). Therefore, there is strong association between the SST pattern and that of the asymmetric distributions of the eastern Pacific precipitation.

The SST mode is symmetric to the Equator in the CP near the dateline, but to the east of 150°W, it has larger positive anomalies north of the Equator than those in the south. This mode of SST variability has been reported as the El Niño Modoki mode (e.g., Ashok et al., 2007; Wang et al., 2016) and is believed to be an internal variability caused by the air-sea interaction in the whole equatorial TP (Yeh et al., 2014). As shown in Figure 3d, the SST PC1 and the El Niño Modoki index (EMI) defined by Ashok et al. (2007) are well correlated with the correlation coefficient cor = 0.76 ($p > 99\%$). In the following, we investigate the cause-effect relationship between this Modoki SST mode and the eastern Pacific precipitation during the boreal spring.

3.2. Remote Impact of SST

In general, warmer SST corresponds to larger moist static energy of near-surface air, which could lead to larger CAPE and more precipitation. This seems to be true in the NEP where the precipitation is significantly correlated with SST (red dots in Figure 4). However, in the SEP, there is no significant relationship between the local SST and precipitation (green dots in Figure 4), implying that the local SST effect cannot explain the interannual variability of precipitation in the SEP. Although the Modoki mode has some hemispheric asymmetries of SST in the eastern Pacific, the overall local SST interannual variation in the SEP is still in phase with the center Pacific SST.

The spatial distribution of SST is found to correlate well with the surface wind convergence during boreal spring in weak El Niño years as shown by a singular value decomposition (SVD) analysis in Figures 5a–5c, which in turn correlates well with precipitation to both sides of the Equator as shown in Figures 5d–5f. The covariance explanation between SST and wind convergence is 37.3%, with time correlation reaching 0.87 and t test probability greater than 99%. The first SVD spatial pattern of SST is almost identical to the first

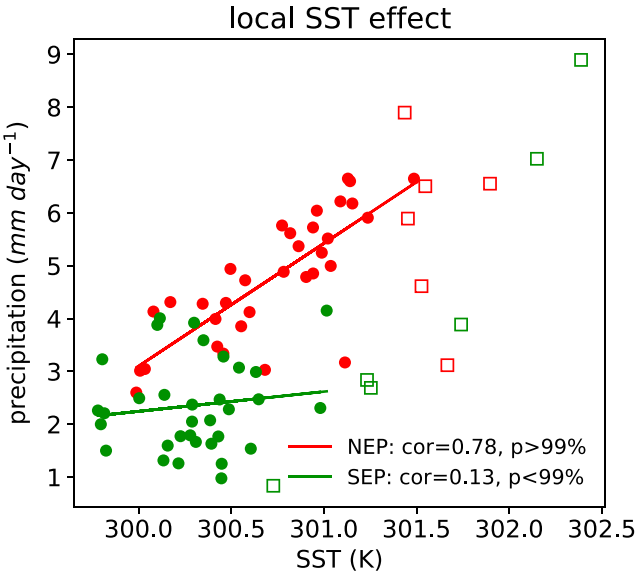

Figure 4. Correlations between the domain averaged precipitation (unit: mm/day) and the local SST (unit: K) for the northeastern equatorial Pacific (red dots and line) and southeastern equatorial Pacific (green dots and line). The correlation coefficients and significance are calculated without the strong El Niño years (squares). SST = sea surface temperature.

EOF pattern of SST shown earlier, suggesting the consistent mechanisms between SST precipitation and SST convergence. The covariance explanation between surface wind convergence and precipitation is 31.5%, with very high time correlation coefficient 0.96 ($p > 99\%$). The first SVD spatial pattern of precipitation is also almost identical to the first EOF pattern of precipitation shown earlier. The spatial pattern of the surface wind convergence shows a significant hemispheric asymmetry in the eastern Pacific, which is similar to the precipitation pattern. Therefore, the surface wind convergence is a key field to explain the association of the interannual modes of SST and precipitation during boreal spring in the weak El Niño years.

The cause-effect relationship of precipitation and surface wind convergence can hardly be separated most of the time. However, we can argue here that the SST spatial distribution can produce the surface wind convergence and therefore the hemispherically asymmetric precipitation. The physical process involves the surface pressure horizontal gradient force induced by the SST distribution, as described in Lindzen and Nigam (1987) and Back and Bretherton (2009). We used the revised linear mixed layer model (MLM) of Back and Bretherton (2009), without considering the momentum entrainment at the top of boundary layer, to reconstruct the surface wind convergence. In the steady state, the surface wind is approximately balanced by the Coriolis force, pressure gradient force, and friction:

$$f\vec{k}\times\vec{V}_S+\frac{1}{\rho_0}\nabla P_S+\varepsilon\vec{V}_S=0 \tag{4}$$

where f is the Coriolis parameter, $\vec{V}_S$ is the surface wind vector, ρ_0 is the constant reference density (1.225 kg/m^3), P_S is the surface pressure, and ε is the friction coefficient (1.5×10^{-5} s^{-1}). Given surface pressure distribution and the friction coefficient, the surface wind and convergence can be solved from equation (4)), which is named as MLM with surface pressure (MLM_Ps).

Furthermore, the surface pressure can be reconstructed based on the geopotential and temperature profile, according to the hydrostatic equation:

$$P_S=P_i\exp\left(\frac{\Phi_i}{R_d\overline{T}}\right) \tag{5}$$

where, P_i = 800 hPa, Φ_i is the geopotential at 800 hPa, R_d is gas constant for dry air, and $\overline{T}$ is the mean air temperature between 800 hPa and surface, which can be estimated as the mean of SST and temperature at 800 hPa (T_i). We assumed the atmospheric MLM to span from the surface to 800 hPa, above which the atmosphere is horizontally homogeneous. The monthly climatologies of Φ_i and T_i are used to reconstruct the surface pressure, so the interannual variation of the derived surface wind convergence represents that of SST only (MLM_SST).

With this simple model, the climatologies of the surface wind convergence in boreal spring can be reconstructed. Both the MLM with surface pressure as input in equation (4) (MLM_Ps) and the SST only model (MLM_SST) can capture the surface wind convergence pattern similar to the distributions with the 10 m wind convergence from ERA-Interim reanalysis data (Figure 6). In particular, the sandwich structure (convergence-divergence-convergence in the NEP-EEP-SEP) in the eastern Pacific is well reproduced by the mixed layer model.

The asymmetric interannual variability of the surface wind convergence in the eastern Pacific can be also explained by the calculated convergence asymmetry from this model. We show in Figure 7a that the hemispheric asymmetry (NEP-SEP) of the surface wind convergence in boreal spring is highly correlated with that of the reconstructed convergence from MLM_Ps (cor = 0.68, $p > 99\%$) and MLM_SST (cor = 0.76, $p > 99\%$), excluding the strong El Niño years. The asymmetry of the precipitation variation is also highly correlated with the wind convergence from the SST-only (MLM_SST) model (Figure 7b). Therefore, the large-scale spatial

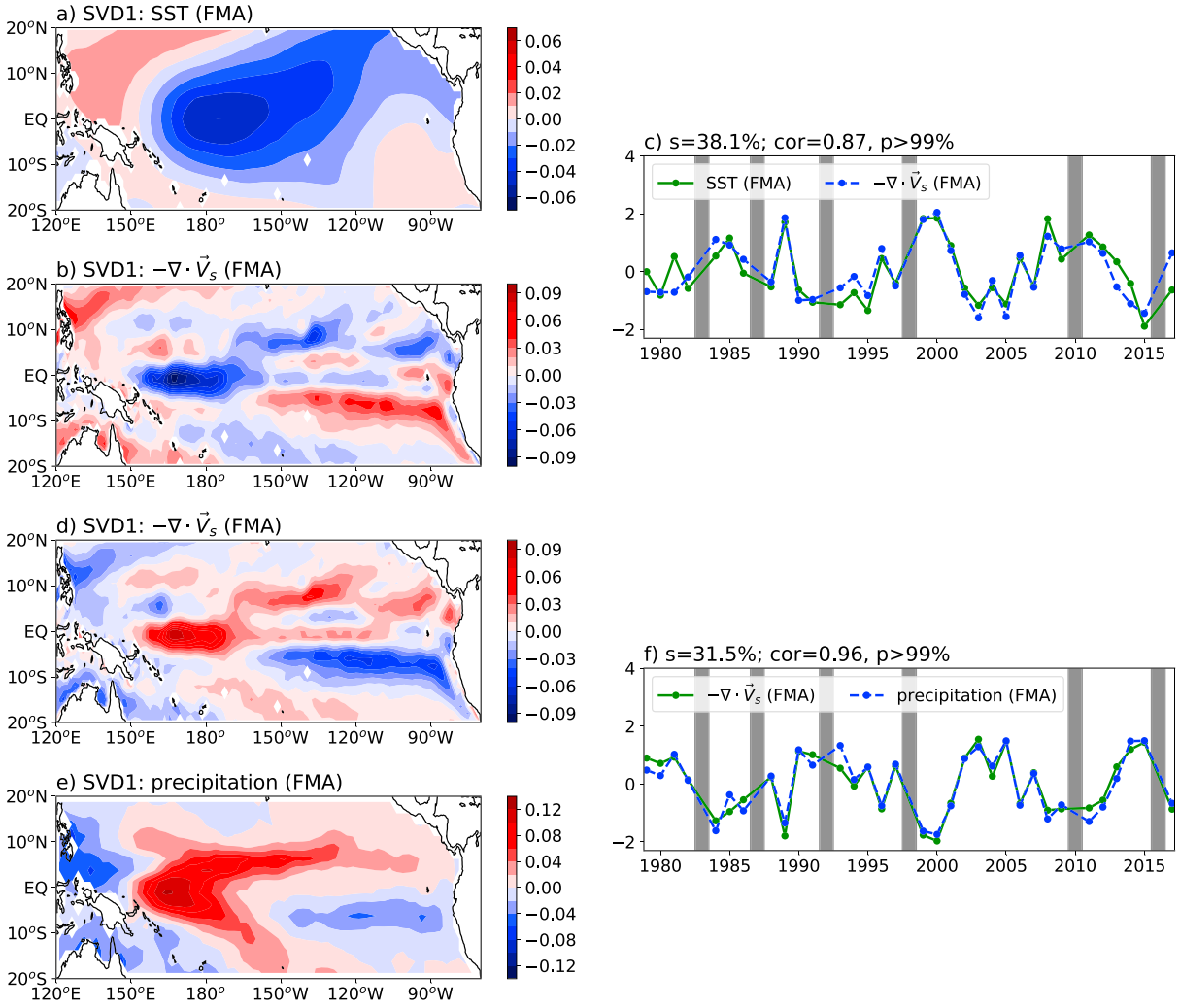

Figure 5. SVD analysis of (a–c) SST convergence and (d–f) convergence precipitation, excluding the strong El Niño years. The first pair of spatial patterns from the SST-convergence SVD analysis is shown in Figure 5a for SST (February, March, and April), and Figure 5b for surface wind convergence (February, March, and April), respectively, with their time series shown in Figure 5c, where the text describes the percentages of variance explained (s), time correlation coefficient (cor), and significance (*p*). The first pair of spatial patterns from the convergence-precipitation SVD analysis is shown in Figure 5d for surface wind divergence (February, March, and April) and (e) for precipitation (February, March, and April), respectively, with their time series shown in Figure 5f. SVD = singular value decomposition; SST = sea surface temperature; FMA = February, March, and April.

pattern of the Modoki mode of SST with the asymmetric SST distribution east of 150°W can cause a surface pressure field that leads to the asymmetry in the wind convergence and precipitation.

Besides wind convergence, another possible remote impact of the CP SST on the eastern Pacific precipitation is through tropospheric temperature. In the tropics, temperature anomaly in the free troposphere follows that of SST in the warmest SST in the western and CP (e.g., Chiang & Sobel, 2002; Wallace et al., 1998). We show in Figure 8 the difference of vertical profiles of temperature between the years in regimes B and C, or the north years and the south years, over the whole TP, NEP, and SEP. The corresponding SST differences are given at the bottom of the figure. As pointed out before, the positive phase of the Modoki mode (regime A) is associated with positive tropospheric temperature anomalies over the whole tropics, including the SEP. There is however a remarkable contrast of the temperature differences over the NEP and SEP. Over the SEP, warming anomaly in the lower troposphere, especially in the lower free troposphere (550–850 hPa), is larger than that of the SST. Over the NEP, warming in the lower troposphere is smaller than that of the SST. Therefore, during the positive phase of the Modoki mode, SST can remotely impact the free tropospheric warm anomalies, leading to different variation of the convective instability and precipitation between the

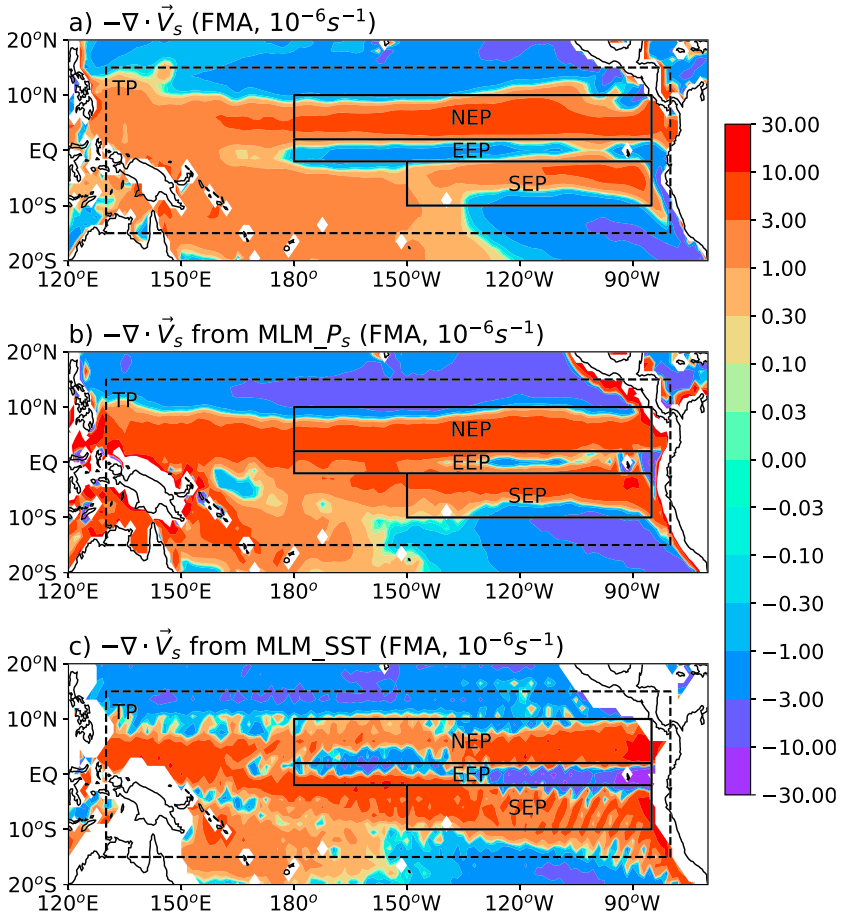

Figure 6. Climatologies of surface wind convergence (unit: 10^{-6} s^{-1}) during boreal spring, derived from (a) ERA-Interim 10 m wind data, (b) MLM_Ps, and (c) MLM_SST.

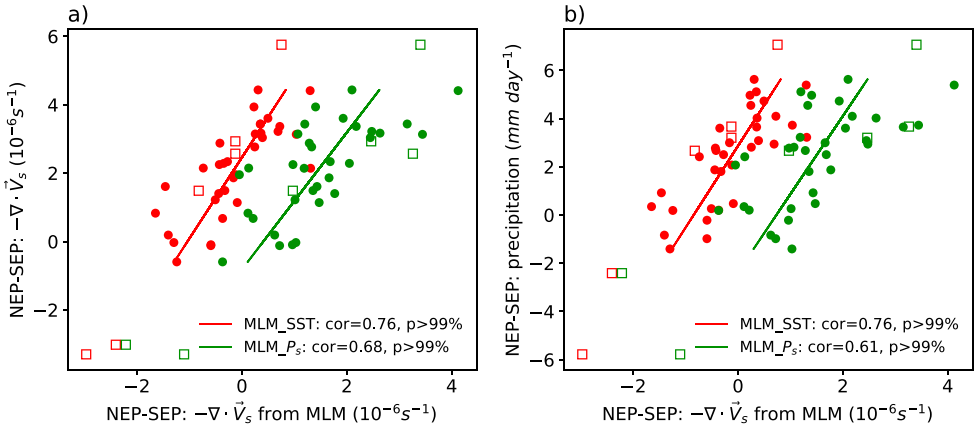

Figure 7. (a) Correlations between the boreal spring asymmetry of surface wind convergence (unit: 10^{-6} s^{-1}), derived from MLM_SST (red dots and line), MLM_Ps (green dots and line) and ERA-Interim data, excluding the strong El Niño years (squares). (b) the same as (a), but correlations with precipitation (unit: mm/day). MLM = mixed layer model; SST = sea surface temperature; NEP = northeastern equatorial Pacific; SEP = southeastern equatorial Pacific; ERA-Interim = European Centre for Medium-Range Weather Forecasts Interim Re-Analysis.

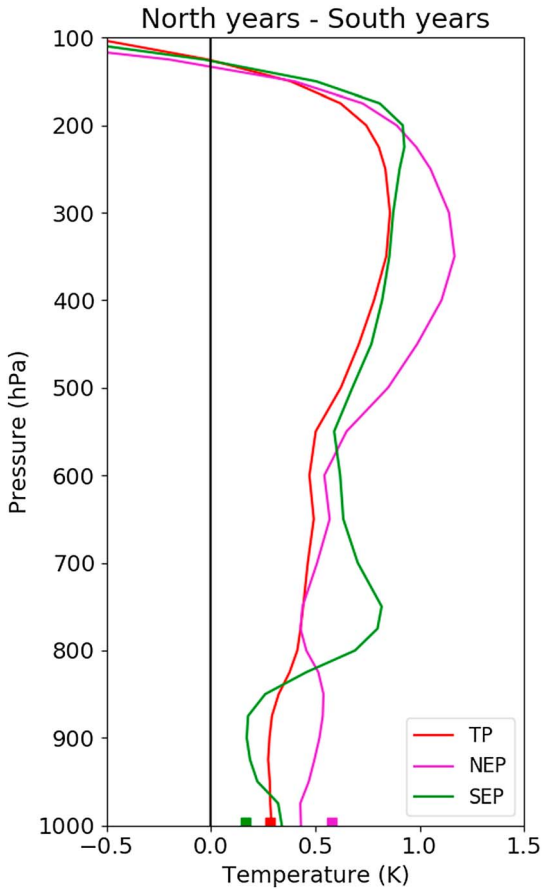

Figure 8. Differences in the vertical temperature profiles and SST (rectangles) between north years and south years in the boreal spring, area-averaged in the tropical Pacific (TP, red), northeastern equatorial Pacific (NEP, purple), and southeastern equatorial Pacific (SEP, green) domains.

SEP and NEP. This remote impact is asymmetric to the Equator, favoring precipitation in NEP while suppressing it in SEP in the positive phase of the Modoki mode.

To understand the relative roles of the two remote processes of SST impact—the surface wind convergence and the vertical stability—on the asymmetric precipitation variation, we conducted three simple numerical experiments with the WRF-ARW. In the control experiment, both the horizontal wind vectors and temperature are relaxed to ERA-Interim reanalysis data with the interannual variation. Water vapor is allowed to change freely in all experiments. The control simulation captured the EOF1 mode of precipitation distribution with the asymmetric distribution that is close to observations in the eastern equatorial Pacific, and the PC1 is nearly identical to the asymmetry index I_a in the simulation (Figures 9a and 9b).

The second experiment is designed to investigate the impact of the atmospheric stability. The atmospheric temperature is relaxed to ERA-Interim reanalysis data with interannual variation, while the winds are relaxed to the monthly climatology. Therefore, the CAPE varies interannually according to the temperature and water vapor. Without the impact of winds, the EOF1 in the interannual variation of precipitation is very different from that of the observation. While PC1 still shows positive correlation with the asymmetry index I_a (Figures 9c and 9d), the explained variance by EOF1 is only 8%. The positive correlation is likely due to the impact of the imposed interannual variation of temperature. This result suggests that fixing the winds largely shuts down the impact of El Niño on precipitation. This is more clearly seen by taking the difference of the precipitation between El Niño and La Niña years (supporting information Figure S1).

The third experiment is performed in which the remote impact of SST on the atmospheric stability is removed by relaxing the atmospheric temperature to fixed climatology of ERA-Interim reanalysis data while the atmospheric winds are relaxed to ERA-Interim reanalysis data with interannual variation. The simulation has nearly the same EOF1 pattern as in the control simulation and in observation, with the corresponding PC1 is highly correlated with the asymmetry index I_a (Figures 9e and 9f). These results suggest that the role of wind divergence is dominant over the vertical stability in the interannual variability of the ITCZ in the eastern TP.

4. Summary and Discussion

We have characterized the interannual variability of boreal spring precipitation over the eastern equatorial Pacific by using two indices and a hierarchical clustering method. We have shown that in weak El Niño years, the interannual variability of ITCZ in the eastern Pacific is primarily associated with the Modoki mode of SST in the CP. The horizontal gradient of the basin-wide SST affects the surface pressure distribution, which then can remotely control the wind convergence and precipitation in the eastern Pacific. In the positive phase of the Modoki mode, the anomaly of the boreal spring ITCZ precipitation is at the north of the Equator in the eastern equatorial Pacific. In the negative phase of the Modoki mode, the anomaly is at south of the Equator.

The above results strongly point to the importance of the dynamical impact of surface wind convergences on the eastern Pacific precipitation. Most current climate models use CAPE as the trigger and closure of convection schemes, without SST gradient or surface convergence as an additional condition. Though the cause and effect between precipitation and surface wind convergence cannot be easily delineated, we have clearly demonstrated that in the eastern Pacific, wind convergence can exist without first considering precipitation forcing. This result hence provides evidence on how convective triggering needs to be parameterized in these models.

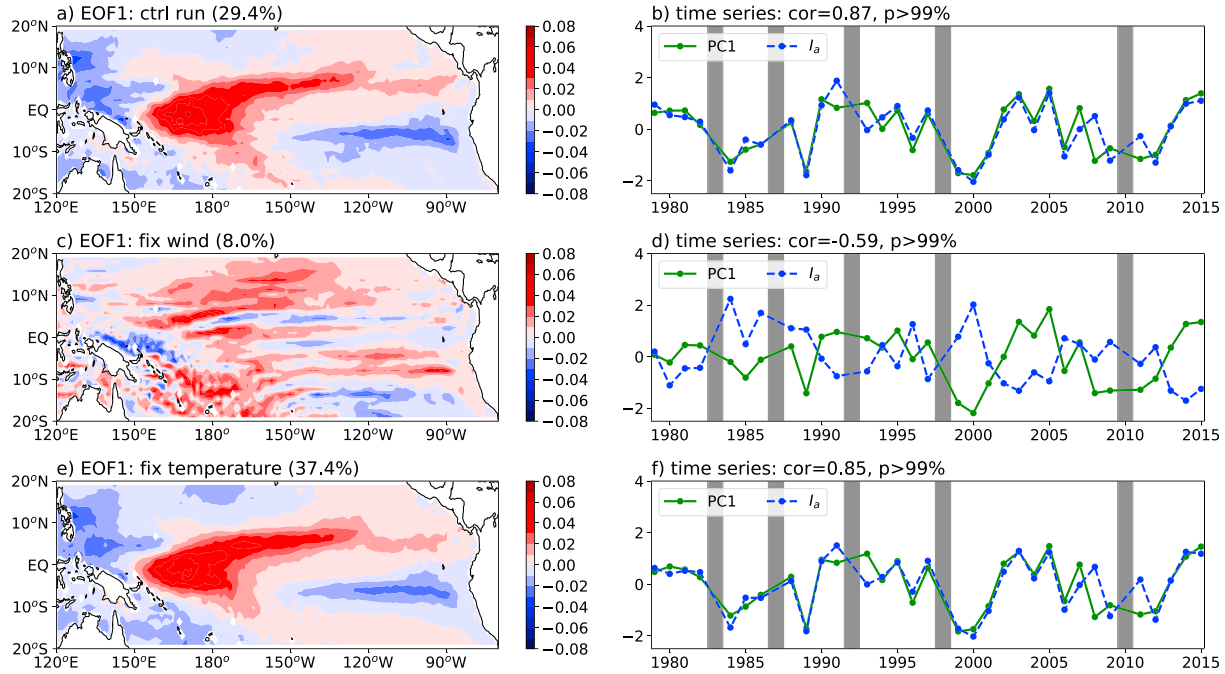

Figure 9. Same as Figure 3 but derived from the WRF simulations: (a) and (b) from the control run; (c) and (d) from the simulation with climatological monthly winds; (e) and (f) from the simulation with climatological monthly temperature. EOF = empirical orthogonal function; PC1 = first principal component.

This study has not addressed what caused the Modoki mode of SST variability. Whether the precipitation anomalies in the eastern Pacific play a role in explaining this SST mode is an open question. The Modoki mode is likely a coupled atmospheric-oceanic variation that involves a large part of the whole TP. The present study only addressed how such a large-scale SST mode can explain the ITCZ variability in the eastern Pacific. A recent study by Xie et al. (2018) independently identified the interannual variability of eastern Pacific precipitation to have a dipole mode. They further argued that this variability is associated with moderate El Niño events. These are consistent with the finding in this study.

Acknowledgments
This research is supported by grant 2016YFB02008 of the National Major Research High-Performance Computing Program of China, the National Science Foundation and the CMDV Project of the Biological and Environmental Research Division in the Office of Sciences of the U.S. Department of Energy (DOE). All the data used for the plots in this paper are provided in the supporting information.

References

Adler, R. F., Huffman, G. J., Chang, A., Ferraro, R., Xie, P.-P., Janowiak, J., et al. (2003). The version 2 Global Precipitation Climatology Project (GPCP) monthly precipitation analysis (1979–present). *Journal of Hydrometeorology*, *4*(6), 1147–1167. https://doi.org/10.1175/1525-7541(2003)004%3C1147:TVGPCP%3E2.0.CO;2

Ashok, K., Behera, S. K., Rao, S. A., Weng, H., & Yamagata, T. (2007). El Niño Modoki and its possible teleconnection. *Journal of Geophysical Research*, *112*, C11007. https://doi.org/10.1029/2006JC003798

Back, L. E., & Bretherton, C. S. (2009). On the relationship between SST gradients, boundary layer winds, and convergence over the tropical oceans. *Journal of Climate*, *22*(15), 4182–4196. https://doi.org/10.1175/2009JCLI2392.1

Chiang, J. C. H., & Sobel, A. H. (2002). Tropical tropospheric temperature variations caused by ENSO and their influence on the remote tropical climate. *Journal of Climate*, *15*(18), 2616–2631. https://doi.org/10.1175/1520-0442(2002)015%3C2616:TTTVCB%3E2.0.CO;2

Grell, G. A., & Dévényi, D. (2002). A generalized approach to parameterizing convection combining ensemble and data assimilation techniques. *Geophysical Research Letters*, *29*(14), 1693. https://doi.org/10.1029/2002GL01531

Gu, G., Adler, R. F., & Sobel, A. H. (2005). The eastern Pacific ITCZ during the boreal spring. *Journal of the Atmospheric Sciences*, *62*(4), 1157–1174. https://doi.org/10.1175/JAS3402.1

Haffke, C., Magnusdottir, G., Henke, D., Smyth, P., & Peings, Y. (2016). Daily states of the March–April East Pacific ITCZ in three decades of high-resolution satellite data. *Journal of Climate*, *29*(8), 2981–2995. https://doi.org/10.1175/JCLI-D-15-0224.1

Huang, B., Thorne, P. W., Smith, T. M., Liu, W., Lawrimore, J., Banzon, V. F., et al. (2016). Further exploring and quantifying uncertainties for Extended Reconstructed Sea Surface Temperature (ERSST) version 4 (v4). *Journal of Climate*, *29*(9), 3119–3142. https://doi.org/10.1175/JCLI-D-15-0430.1

Hwang, Y. T., & Frierson, D. M. W. (2013). Link between the double-Intertropical Convergence Zone problem and cloud biases over the Southern Ocean. *Proceedings of the National Academy of Sciences of the United States of America*, *110*(13), 4935–4940. https://doi.org/10.1073/pnas.1213302110

Li, G., & Xie, S. P. (2014). Tropical biases in CMIP5 multimodel ensemble: The excessive equatorial Pacific cold tongue and double ITCZ problems. *Journal of Climate*, *27*(4), 1765–1780. https://doi.org/10.1175/JCLI-D-13-00337.1

Lindzen, R. S., & Nigam, S. (1987). On the role of sea surface temperature gradients in forcing low level winds and convergence in the tropics. *Journal of the Atmospheric Sciences*, *44*(17), 2418–2436. https://doi.org/10.1175/1520-0469(1987)044%3C2418:OTROSS%3E2.0.CO;2

Mason, S. J., & Goddard, L. (2001). Probabilistic precipitation anomalies associated with ENSO. *Bulletin of the American Meteorological Society*, *82*(4), 619–638. https://doi.org/10.1175/1520-0477(2001)082%3C0619:PPAAWE%3E2.3.CO;2

Masunaga, H., & L'Ecuyer, T. S. (2010). The southeast Pacific warm band and double ITCZ. *Journal of Climate*, *23*(5), 1189–1208. https://doi.org/10.1175/2009JCLI3124.1

Mechoso, C. R., Robertson, A. W., Barth, N., Davey, M. K., Delecluse, P., Gent, P. R., et al. (1995). The seasonal cycle over the tropical Pacific in coupled ocean–atmosphere general circulation models. *Monthly Weather Review*, *123*(9), 2825–2838. https://doi.org/10.1175/1520-0493(1995)123%3C2825:TSCOTT%3E2.0.CO;2

Oueslati, O., & Bellon, G. (2015). The double ITCZ Bias in CMIP5 models: Interaction between SST, large-scale circulation and precipitation. *Climate Dynamics*, *44*(3-4), 585–607. https://doi.org/10.1007/s00382-015-2468-6

Ropelewski, C. F., & Halpert, M. S. (1987). Global and regional scale precipitation patterns associated with the El Niño/Southern Oscillation. *Monthly Weather Review*, *115*(8), 1606–1626. https://doi.org/10.1175/1520-0493(1987)115%3C1606:GARSPP%3E2.0.CO;2

Simmons A., Uppala, S., Dee, D., & Kobayashi, S. (2007). Era-Interim: New ECMWF reanalysis products from 1989 onwards. In *ECMWF Newsletter* (Vol. 110, pp. 25–35). Reading, UK: European Centre for Medium-Range Weather Forecasts.

Skamarock, W. C., Klemp, J. B., Dudhia, J., Gill, D. O., Barker, D. M., Duda, M. G., et al. (2008). A description of the Advanced Research WRF version 3 (Tech. Note NCAR/TN-475+STR). Boulder, CO: National Center for Atmospheric Research.

Wallace, J. M., Rasmusson, E. M., Mitchell, T. P., Kousky, V. E., Sarachik, E. S., & von Storch, H. (1998). On the structure and evolution of ENSO-related climate variability in the tropical Pacific: Lessons from TOGA. *Journal of Geophysical Research*, *103*, 14, 241–14,259. https://doi.org/10.1029/97JC02905

Wang, C., Deser, C., Yu, J.-Y., DiNezio, P., & Clement, A. (2016). El Niño-Southern Oscillation (ENSO): A review. In P. Glymn, D. Manzello, & I. Enochs (Eds.), *Coral reefs of the eastern Pacific* (pp. 85–106). Berlin, Germany: Springer.

Xie, S., Peng, Q., Kamae, Y., Zheng, X., Tokinaga, H., & Wang, D. (2018). Eastern Pacific ITCZ dipole and ENSO diversity. *Journal of Climate*. https://doi.org/10.1175/JCLI-D-17-0905.1

Yang, W., & Magnusdottir, G. (2016). Interannual signature in daily ITCZ states in the East Pacific in boreal spring. *Journal of Climate*, *29*(22), 8013–8025. https://doi.org/10.1175/JCLI-D-16-0395.1

Yeh, S.-W., Kug, J.-S., & An, S.-I. (2014). Recent progress on two types of El Niño: Observations, dynamics, and future changes. *Asia-Pacific Journal of Atmospheric Sciences*, *50*(1), 69–81. https://doi.org/10.1007/s13143-014-0028-3

Zhang, C. (2001). Double ITCZs. *Journal of Geophysical Research*, *106*, 11,785–11,792. https://doi.org/10.1029/2001JD900046

Zhang, X., Liu, H., & Zhang, M. (2015). Double ITCZ in coupled ocean-atmosphere models: From CMIP3 to CMIP5. *Geophysical Research Letters*, *42*, 8651–8659. https://doi.org/10.1002/2015GL065973